energies

MDPI

Article

A Fuzzy-PID Scheme for Low Speed Control of a Vehicle While Going on a Downhill Road

Liqiang Jin [1], Ronglin Zhang [1,*], Binghao Tang [2] and Hao Guo [3]

[1] State Key Laboratory of Automotive Simulation and Control, Jilin University, Changchun 130022, China; jinlq@jlu.edu.cn
[2] Zhejiang Asia-Pacific Mechanical & Electronic Co., Ltd., Hangzhou 311203, China; tbh@apg.cn
[3] Zhejiang Geely Automobile Research Institute Co., Ltd., Ningbo 315336, China; gh89125@163.com
* Correspondence: ronglinzhang@126.com; Tel.: +86-130-2912-1298

Received: 18 April 2020; Accepted: 22 May 2020; Published: 1 June 2020

Abstract: We explored a vehicle hill descent control (HDC) system based on an electronic stability program (ESP) and applied this system to brake cars. The experimental results reveal that our system can effectively reduce the workload of a driver during a downhill journey. In the first phase of our work, the control strategy of the HDC system based on fuzzy-PID (Proportion Integral Differential) was built by MATLAB/Simulink. Then, the co-simulation based on MATLAB/Simulink, CarSim and AMESim was carried out. Finally, a real vehicle test was conducted to further verify the feasibility of the strategy. A series of simulation experiments and real vehicle tests show that the HDC system can assist the driver to control the vehicle while driving downhill at low speed, thus effectively improving the safety of the vehicle and reducing the workload of driver.

Keywords: HDC; ESP; Fuzzy-PID; co-simulation; real vehicle tests

1. Introduction

According to statistics, more than 1.3 million people lose their lives and more than 50 million people are seriously injured every year as a consequence of road accidents [1]. Although scientists have used various methods to solve car safety problems and have achieved some success, there is still a long way to go to improve car safety [2]. Among these road traffic crashes, the death rate on downhill roads is much higher than the average rates [3]. Research data shows that the accident rate increases with the increase of the road slope; the higher the slope, the more obvious it is [4]. Thus, downhill safety is an extremely important topic in vehicle safety research. As we all know, when driving on a long steep downhill road, maintaining the vehicle speed in a certain range by using a reliable brake system can effectively reduce the workload of driver, which ensures that the driver puts more attention on the steering vehicle [5]. In the past decades, many new technologies have been applied to improve the braking safety of vehicles on downhill roads, such as hydraulic braking systems [6,7], auxiliary braking systems for the engine [8,9], retarder auxiliary braking systems [10,11], and regenerative braking [12]. However, an auxiliary braking system for the engine provides limited braking torque, which cannot be controlled accurately [13–16]. Retarder braking systems have slow responses and will lead to heat recession after long-term operation [17,18]. Regenerative braking not only provides limited braking torque, but also can only be applied to electric vehicles. Therefore, it is highly desirable to find an efficient dynamic control system to improve the downhill braking performance of vehicles.

Stable and reliable braking power can be provided by an ESP within the vehicle. Recently, various value-added functions based on ESP hydraulic circuit systems have made rapid development. These additional functions have a great advantage in providing more comfortable and convenient driving experience for the driver by automatically applying the brakes [19]. Among various additional

functions, the HDC system has been found to be the most valuable function, because it can maintain vehicle speed in a certain range by automatically applying the brakes. Besides, the HDC system is also helpful in reducing the workload of the driver and helps the driver pay more attention to steering the vehicle.

Here, the fuzzy-PID control method is adopted to build up the HDC system. As we all know, PID controllers are widely used in the automotive field due to their simple application and suitable performance. However, in the case of strong nonlinearity of the vehicle system, the efficacy of simple PID controllers is not ideal. In addition, PID controller with fixed parameters greatly limits their application and effectiveness in a variety of real-world environments [20]. So far, it is of great urgency to find an efficient and simple control method to make up for these deficiencies. Fuzzy controllers logic has emerged as a complement to conventional strict methods, as the fuzzy logic based controllers can handle the uncertainty; however, normal fuzzy control cannot eliminate the steady state error efficiently [21]. Fuzzy-PID controllers combine the advantages of PID controllers and fuzzy controllers [22–24]. On the one hand, the performance of PID controllers can be enhanced via a fuzzy logic assisted controller by automatically changing the controller parameters. On the other hand, the steady state error can be controlled in a small range. Further more, the actual speed of the vehicle is fed back to fuzzy-PID controller in real time. The controller adjusts the target braking torque in real time to make the vehicle reach the target speed according to the difference of the target speed and actual speed. The change of the resistances related to the vehicle tractions and the slope of the terrain will lead to the change of the vehicle actual speed, so the complex interactions between vehicle user infrastructure can be simplified [25–27].

In this paper, the whole vehicle simulation model was established based on CarSim software; the HDC strategy simulation model were built up through MATALB/Simulink software by using control theories of fuzzy-PID logic control; the fuzzy logic control strategy were conducted through the development of fuzzy membership functions in MATALB's Fuzzy Logic Toolbox and Simulink. A hydraulic brake system simulation model was established via AMESim software. The PID controller has been designed to be compared with fuzzy-PID controllers. The characteristics and effects of control strategy were further validated and analyzed according to the CarSim-AMESim-Simulink co-simulation. In order to verify the feasibility of the algorithm, a real vehicle test was conducted.

2. Methodology

When the HDC is motivated, the target vehicle speed is calculated, which is used by the control logic of fuzzy-PID theories as a control variable with actual vehicle speed that is from Vehicle model built via CarSim. The result of the control strategy is target braking pressure. The different valves will be motivated to achieve the target pressure in AMESim circumstance. The specific process is shown in Figure 1a,b (The meaning of the symbols are shown in Table 1).

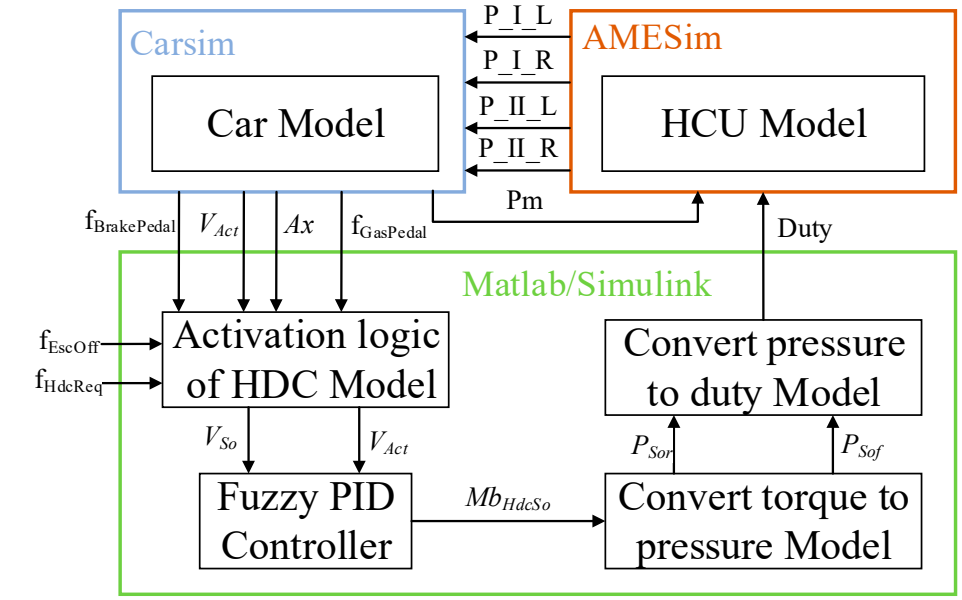

(**a**)

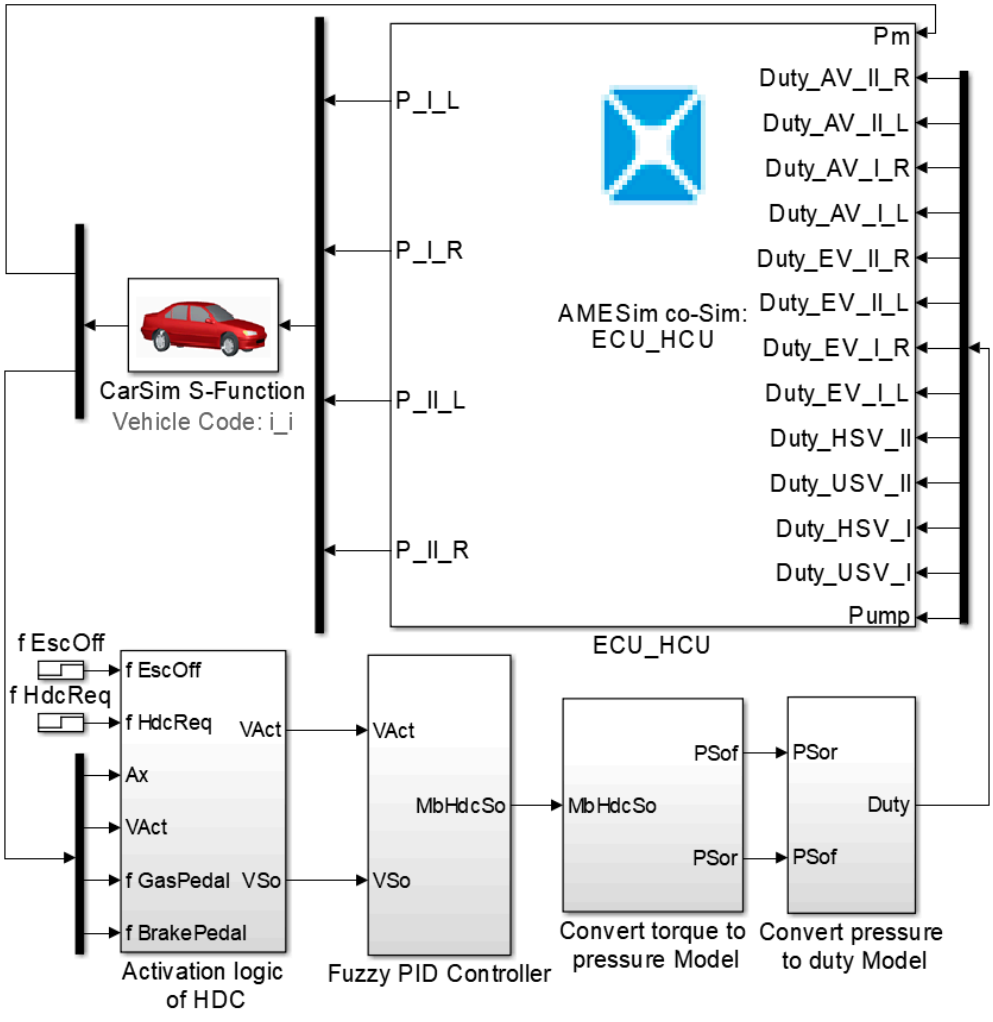

(**b**)

Figure 1. (**a**) Co-simulation framework, (**b**) co-simulation process.

2.1. The HDC Strategy

2.1.1. Activation Logic of HDC

Figure 2 (The meaning of the symbols are shown in Table 1) reveals the activation logic of the HDC. In this system, if HDC is requested and the ESP opened during driving downhill, the HDC will be motivated when the vehicle speed goes below the maximum threshold. HDC will be closed in the following four cases: 1. the HDC turned off; 2. the ESC turned off; 3. vehicle downhill ended; 4. the activation time reaches the maximum value. These designs effectively prevent the HDC system from being motivated on a flat road or running for too long time. Besides, the driver can turn it off at any time. In this logic the initial target speed is $C_{VSoHdcInt}$, it will be updated when the driver is detected pushing the brake pedal or the accelerator pedal. It is worth noting that the target speed limited between $C_{VSoHdcMin}$ and $C_{VSoHdcMmx}$.

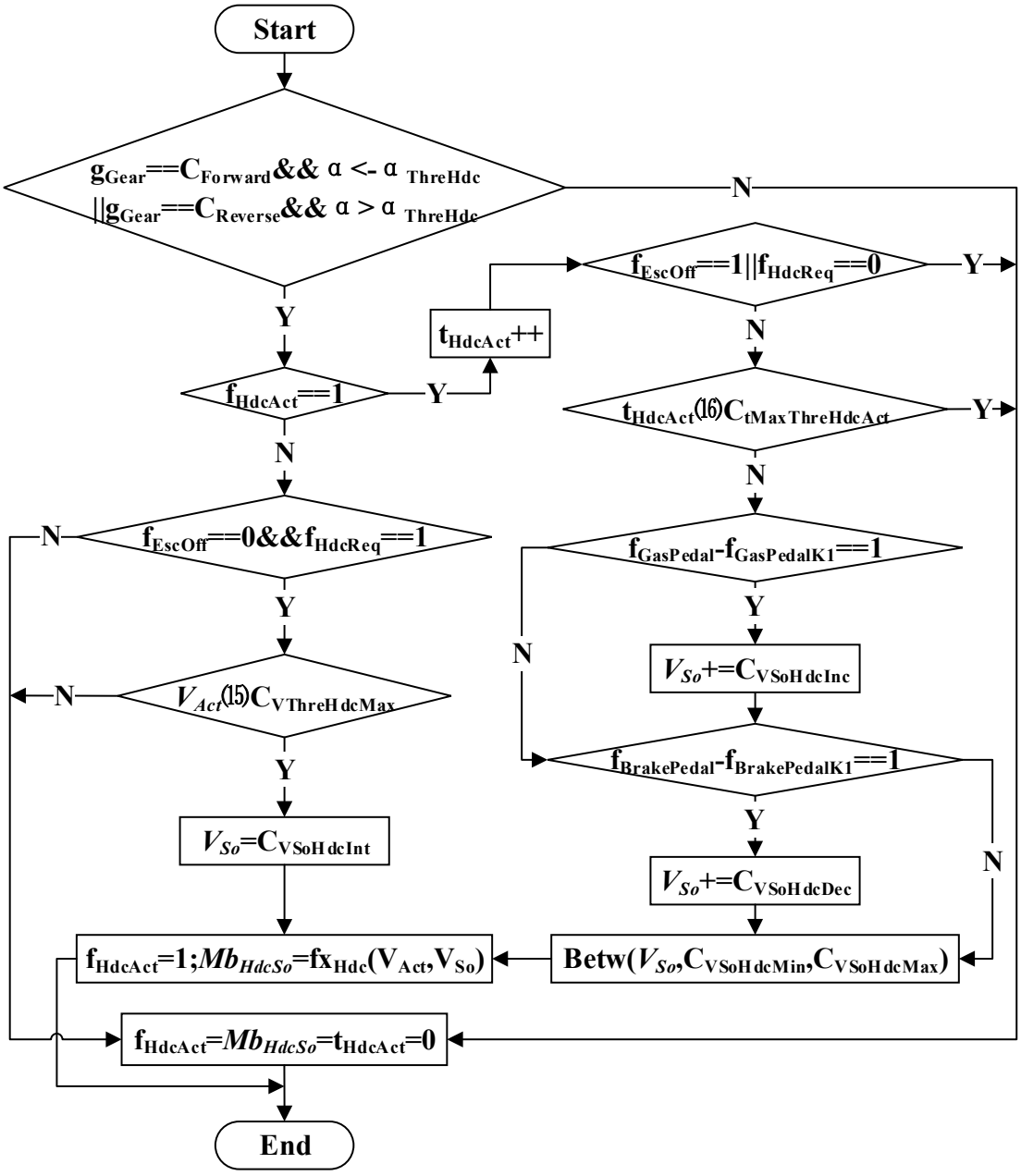

Figure 2. Activation logic of HDC.

Table 1. List of main symbols in this article.

Symbol	Description	Unit
Ax/g	The measured/Gravitational acceleration	m/s^2
g_{Gear}	The gear of vehicle	1
$C_{ForWard}/C_{Reverse}$	Forward/Reverse gears	1
α	The slope of ramp (The value is positive when the car's nose is uphill and it is negative when downhill.)	100%
θ	The angle of ramp	rad
$\alpha_{ThreHdc}$	The threshold of slope of ramp	100%
f_{HdcAct}	The activation flag of HDC (The value is 1 when the HDC is motivated and 0 when HDC is shut down)	1
f_{EscOff}	The close flag of ESC (The value is 1 when the ESC is open and 0 when ESC is shut down)	1
f_{HdcReq}	The requirement flag of HDC (The value is 1 when the HDC is requested and 0 when it is not)	1
f_{xHdc}	The function to calculate the target brake torque	1
hg	The height of vehicle center of mass	m
L	Wheel base	m
L_f/L_r	The distance between the front/rear axle and the center of mass	m
m	The mass of vehicle	Kg
V_{Act}/V_{So}	Actual/Target vehicle speed	km/h
$C_{VThreHdcMax}$	The maximum vehicle speed that HDC can be motivated	km/h
$C_{VSoHdcInt}$	The initial target speed when HDC is motivated	km/h
Mb_{HdcSo}	Target brake torque	Nm
P_w	Actual brake pressure of wheel cylinder (From the pressure sensor)	bar
P_{SoAVe}	Average target brake pressure	bar
P_{Sof}/P_{Sor}	The target pressure of the front rear axle	bar
P_{Maxf}/P_{Maxr}	The maximum pressure that the front/rear axle can withstand	bar
P_m	Master cylinder pressure	bar
R_f/R_r	The front/rear wheel radius	m
u	The road adhesion coefficient	1
$C_{PThrInc}$	The threshold to increase the pressure of wheel cylinder	bar
$C_{tMaxThreHdcAct}$	Maximum duration of HDC operation	s
f_{Motor}	The motor start flag	1
$f_{GasPedal}/f_{BrakePedal}$	The flag of acceleration/brake pedal (The value is 1 when the pedal is pushed and 0 when the pedal is released)	1
$f_{GasPedalK1}/f_{BrakePedalK1}$	The flag of acceleration/brake in the Last Cycle	1
$C_{VSoHdcInc}/C_{VSoHdcDec}$	Increment/Decrement value of target speed	km/h
$C_{VSoHdcMin}/C_{VSoHdcMax}$	Minimum/Maximum target vehicle speed	km/h
$K_p/K_i/Kd$	The proportional/integral/differential parameter	1
Cp_f/Cp_r	The front /rear axle ratio of brake torque to brake pressure	Nm/bar
$Duty_{USV}/Duty_{HSV}$	The duty of USV/HSV	%
HDC	Hill descent control	1
PID	Proportion Integral Differential	1
ESP	Electronic stability program	1
E	The difference between the target speed and the actual speed	1
EC	The differential of the difference between the target speed and the actual speed	1
HCU	Hydraulic control unit	1
ECU	Electronic control unit	1
CAN	Controller area network	1

2.1.2. Fuzzy-PID Logic Control of HDC

The fxHdc is the function to calculate the target brake torque, which is designed by feedback control of fuzzy-PID logic. The block diagram of the proposed self tuning fuzzy-PID type controller is given in Figure 3 (The meaning of the symbols are shown in Table 1). According to the need of fuzzy logic controller design, the quantificational field of fuzzy variables E and EC is defined as follows:

input of Fuzzy system are E (the difference between the target speed and the actual speed) and EC (differential of the difference between the target speed and the actual speed). Output of Fuzzy system are Kp (the proportional parameter), Ki (the integral parameter) and Kd (the differential parameter).

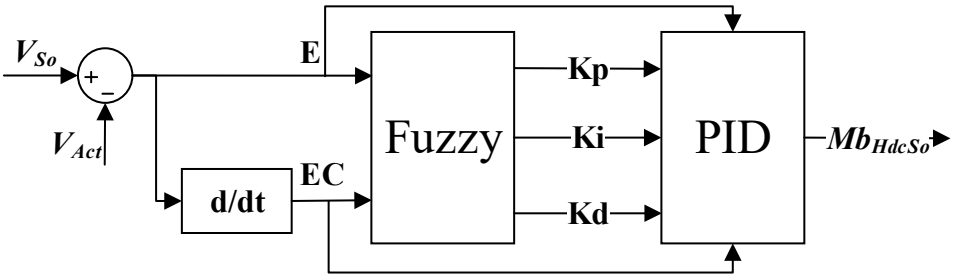

Figure 3. Structure of proposed fuzzy-PID controller.

The fuzzy sets of E and EC are defined as {NB, NM, ZO, PM, PB}, and their universes are defined as [–20, 10] and [–10, 10]. The membership functions of E and EC is brought in Figure 4a,b, and their division is shown in Tables 2 and 3. The fuzzy sets of Kp, Ki and Kd are defined as {O, S, M, B}, and their universes are defined as [0, 500] and [0, 20] and [0, 10]. The membership functions of Kp, Ki and Kd are revealed in Figure 4c–e, and their division is shown in Tables 4–6. The rules of fuzzy logic control can be expressed by conditional statement of "if … then … ", which represent decision result derived from many change premises.

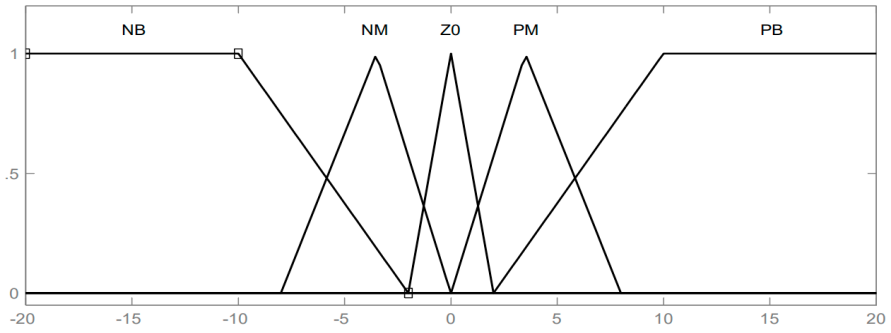

(**a**)

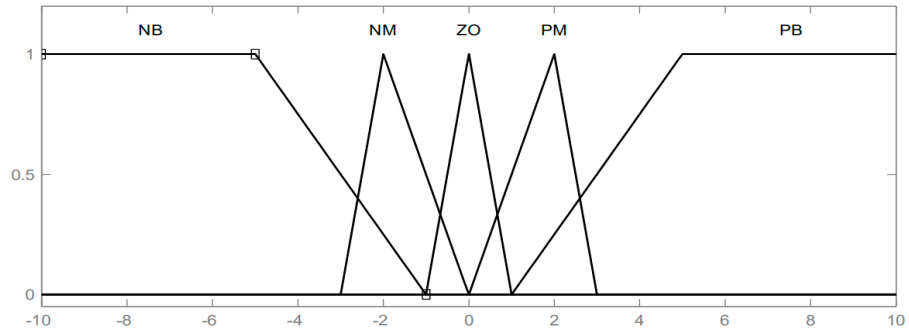

(**b**)

Figure 4. *Cont.*

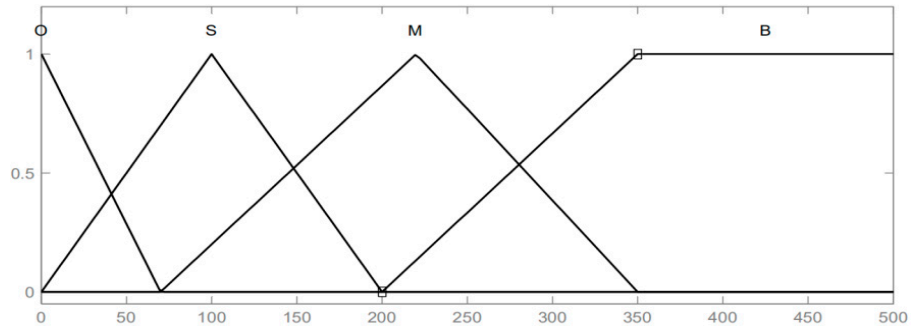

(**c**)

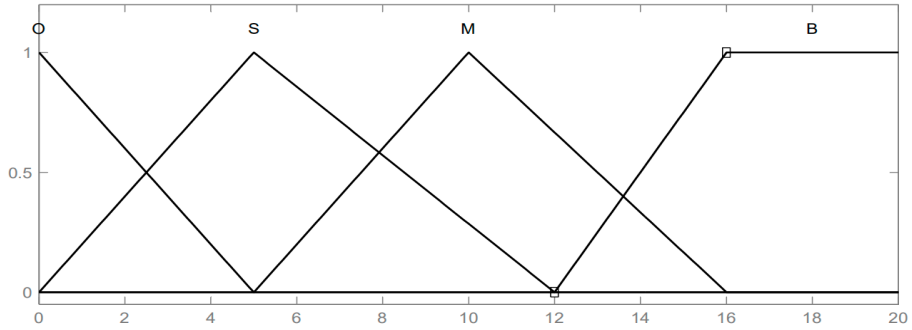

(**d**)

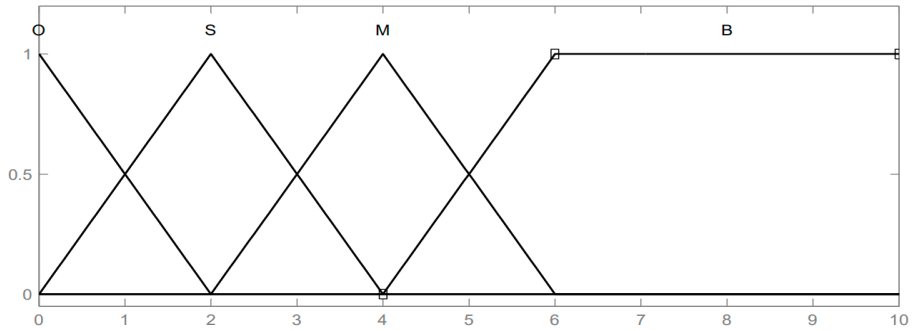

(**e**)

Figure 4. Membership functions of E (**a**), EC (**b**), Kp (**c**), Ki (**d**) and Kd (**e**), respectively.

In general, fuzzy logic control form is used to express those rules, as shown in Tables 7–9. Wherein, NB represent Negative Big, NM is Negative Medium, NS is Negative Small, ZE is Almost Zero, PS is Positive Small, PM is Positive Medium, PB is Positive Big, O is Almost Zero, S is Small, M is Medium, B is Big. In this system, the output of the fuzzy system will be used as a parameter of the PID controller, and the final output of the fuzzy-PID controller is the target brake torque.

Table 2. Division of universe E.

Membership Functions	NB	NM	ZO	PM	PB
Range	[–30 –20 –10 –2]	[–8 –3.5 0]	[–2 0 2]	[0 3.5 8]	[2 10 20 30]

Table 3. Division of universe EC.

Membership Functions	NB	NM	ZO	PM	PB
Range	[–20 –10 –5 –1]	[–3 –2 0]	[–1 0 1]	[0 2 3]	[1 5 10 20]

Table 4. Division of universe Kp.

Membership Functions	O	S	M	B
Range	[–200 0 70]	[0 100 200]	[70 220 350]	[200 350 610 775]

Table 5. Division of universe Ki.

Membership Functions	O	S	M	B
Range	[–8 0 5]	[0 5 12]	[5 10 16]	[12 16 24 30]

Table 6. Division of universe Kd.

Membership Functions	O	S	M	B
Range	[–4 0 2]	[0 2 4]	[2 4 6]	[4 6 10 20]

Table 7. Kp rules of fuzzy control.

EC Kp E	NB	NM	ZO	PM	PB
NB	S	S	M	S	O
NM	M	M	B	M	M
ZO	B	M	B	M	B
PM	M	M	B	M	M
PB	S	S	M	S	S

Table 8. Ki rules of fuzzy control.

EC Kp E	NB	NM	ZO	PM	PB
NB	O	O	S	O	O
NM	O	S	M	S	O
ZO	S	M	B	M	S
PM	O	S	M	S	O
PB	O	O	S	O	O

Table 9. Kd rules of fuzzy control.

EC Kp E	NB	NM	ZO	PM	PB
NB	O	M	B	M	O
NM	S	S	M	S	S
ZO	O	O	S	O	O
PM	S	S	M	S	S
PB	O	M	B	M	O

2.1.3. PID Logic Control of HDC

To compare the proposed fuzzy-PID controller, we set up the PID controller. The corresponding scheme is given in Figure 5 (The meaning of the symbols are shown in Table 1). In this system, inputs of the controller are E and EC, and its output is target brake torque (similar to fuzzy-PID controller). By contrast with the fuzzy-PID controller, the PID controller is carried out with fixed parameters (Kp, Ki, Kd are constant).

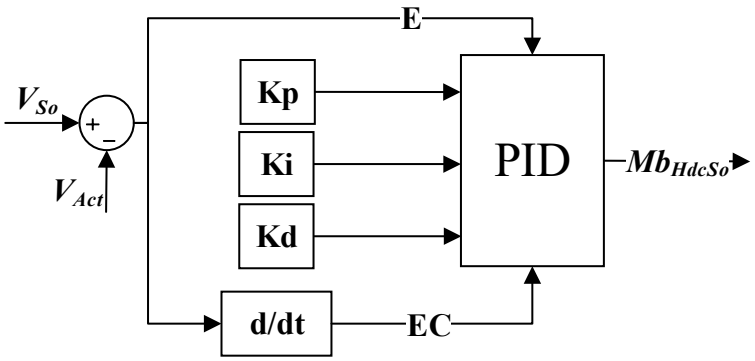

Figure 5. Structure of proposed PID controller.

2.2. Convert Target Torque of HDC to Pressure

The brake torque is proportional to the brake pressure and the proportional relation is as follows:

$$P_{SoAve} = Mb_{HdcSo}/(Cp_f + Cp_r) \tag{1}$$

If the required pressure is evenly distributed between the front and rear axles, the target pressure of the front and rear axle will be the same as P_{SoAve}. However, the maximum pressure that can be applied to the front and rear axles are usually different when the vehicle goes downhill, because the load of the rear axle will be transferred to the front axle. The maximum pressure that the front axle can withstand is shown as Formula (2), The maximum pressure of the rear axle is shown as Formula (3).

$$P_{Maxf} = (m{\cdot}g\frac{l_r}{L} - m{\cdot}\frac{h_g}{L}{\cdot}A_x){\cdot}u{\cdot}R_f/Cp_f \tag{2}$$

$$P_{Maxr} = (m{\cdot}g\frac{l_f}{L} + m{\cdot}\frac{h_g}{L}{\cdot}A_x){\cdot}u{\cdot}R_r/Cp_r \tag{3}$$

We suppose that the road surface is high adhesion, and the road adhesion coefficient u is "1". There are only three types of the relationships between the pressure and the target pressure of the front and rear axle are shown in the following formula:

A. If $P_{SoAve} \le P_{Maxf}$ and $P_{SoAve} \le P_{Maxr}$,

$$P_{Sof} = P_{SoAve} \tag{4}$$

$$P_{Sor} = P_{SoAve} \tag{5}$$

B. If $P_{SoAve} \ge P_{Maxf}$ and $P_{SoAve} < P_{Maxr}$,

$$P_{Sof} = P_{Maxf} \tag{6}$$

$$P_{Sor} = (P_{SoAve} - P_{Maxf}){\cdot}Cp_f/Cp_r + P_{SoAve} \tag{7}$$

C. If $P_{SoAve} < P_{Maxf}$ and $P_{SoAve} \ge P_{Maxr}$,

$$P_{Sof} = (P_{SoAve} - P_{Maxr}){\cdot}Cp_r/Cp_f + P_{SoAve} \tag{8}$$

$$P_{Sor} = P_{Maxr} \tag{9}$$

It will indicates the slope is too large and the vehicle cannot descend normally if $P_{SoAve} > P_{Maxf}$ and $P_{SoAve} > P_{Maxr}$. The meaning of the symbols above are shown in Table 1.

2.3. Convert Target Pressure of HDC to the Duty of Valves

The schematic diagram of the HCU (hydraulic control unit) and the model of the HCU built in AMESim are shown in Figures 6 and 7, respectively. HCU consists of two normally open and two closed type solenoid valves. USV (USV_I, USV_II) and EV (EV_I_L, EV_I_R, EV_II_L, EV_II_R) are normally the open linear solenoid valve, which will be closed when energized. The pressure required to open USV and EV is proportional to the electromagnetic force from the electromagnetic coil. HSV (HSV_I, HSV_II) and AV (AV_I_L, AV_I_R, AV_II_L, AV_II_R) are the normally closed switching solenoid valve, and their states (closed or opened) are controlled electronically. The working principle of the wheel cylinder to establish pressure is as follows. The brake fluid flows through the valve USV and EV from the master cylinder to the wheel cylinders when the driver pushes the brake pedal. While the vehicle is braked without the intervention of the driver, the electromagnetic coil USV will be energized and the valve of HSV will be opened; at the same time, the motor will be motivated, the brake fluid flows through the valve HSV and EV from the master cylinder to the wheel cylinders.

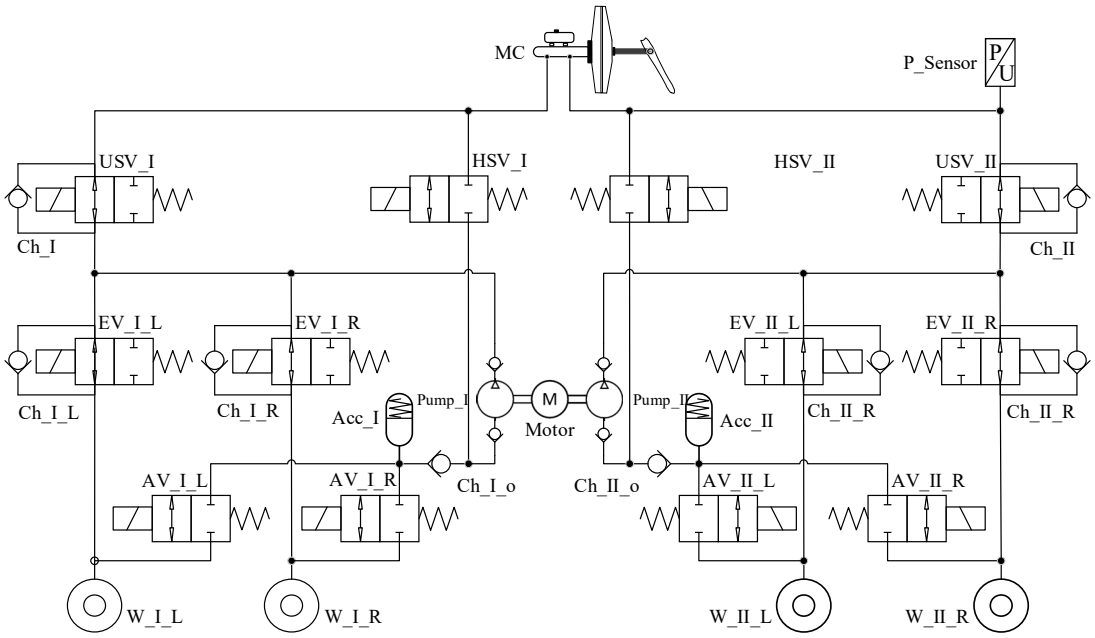

Figure 6. Schematic diagram of hydraulic control unit (HCU).

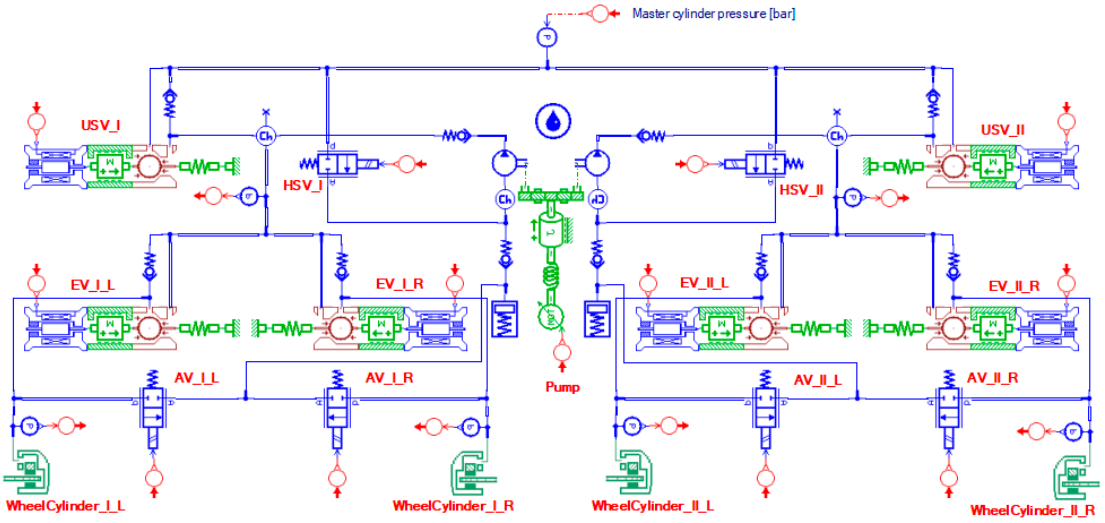

Figure 7. The model of HCU built in AMESim.

Pressure corresponding to the different duty of USV is given in Figure 8. The pressure that wheel cylinders can reach is proportional to the duty of the USV, and 100% corresponds to the current of 2 amperes of the electromagnetic coil. As we all know, the greater the current, the greater the electromagnetic force. Therefore, we can convert the target pressure to the load of the USV to brake the vehicle at a certain brake pressure.

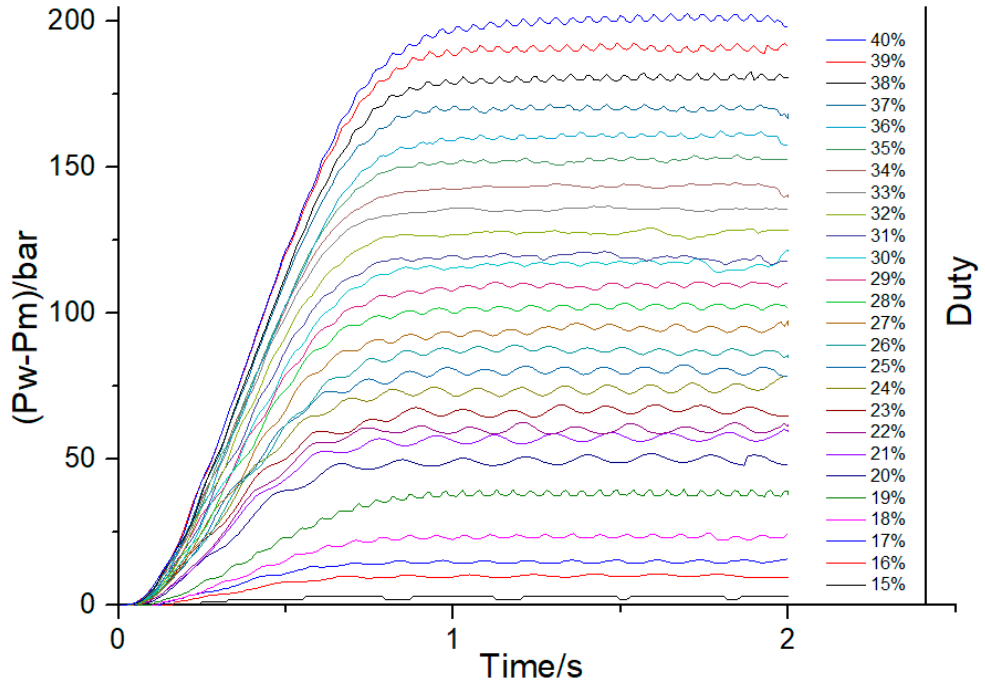

Figure 8. Pressure corresponding to different duty of linear solenoid valve (USV).

The control logic of USV, HSV and Motor are shown in Figure 9 (The meaning of the symbols are shown in Table 1). In this logic, it is worth noting that the USV, HSV and motor will be uncontrolled if Pm is bigger than PSo. If the difference between PSo and Pw is greater than CPThreInc, the pressure of the wheel cylinder must be increased by starting the motor, opening the HSV and closing the USV (the duty of USV can be found from Figure 8). If the difference between PSo and Pw is lower than CPThreInc, the pressure of the wheel cylinder can be adjusted by simply adjusting the duty of USV.

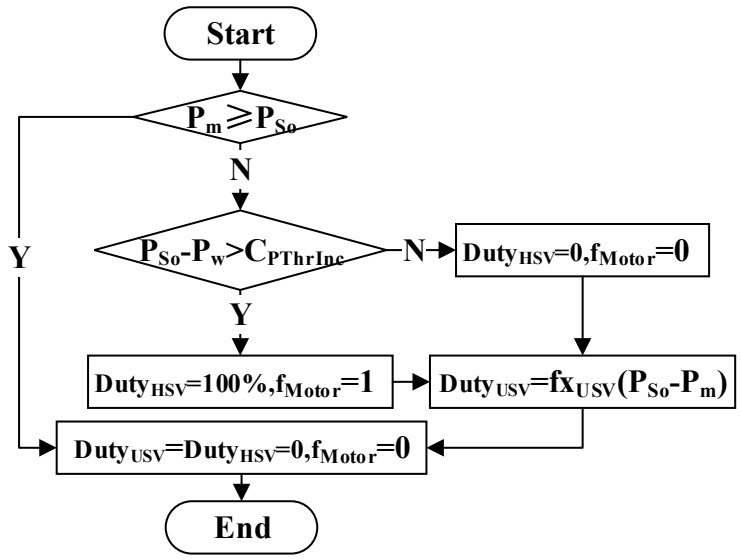

Figure 9. The control logic of USV, switching solenoid valve (HSV) and motor.

3. Simulations and Analysis

In order to further confirm the rationality and feasibility of our model algorithm, a series of simulation experiments were carried out. All simulation tests were performed in MATLAB/Simulink, CarSim and AMESim co-simulation environment.

CarSim is a simulation software specifically for vehicle dynamics. The CarSim user interface is shown in Figure 10, it mainly includes Test Specifications, Run control with Simulink and Results (Post Processing). The vehicles parameters and simulation conditions can be defined in Test Specifications; Simulation solution configurations is set in Run control with Simulink; Results (Post Processing) Can display 3D animation and draw simulation curves.

Vehicle parameters, road information and simulation conditions are set in CarSim in advance, the CarSim can simulate real car movement, the actual speed and acceleration of the vehicle will be output when the brake pressure of the wheel cylinders are input to the CarSim.

The test results are as follows:

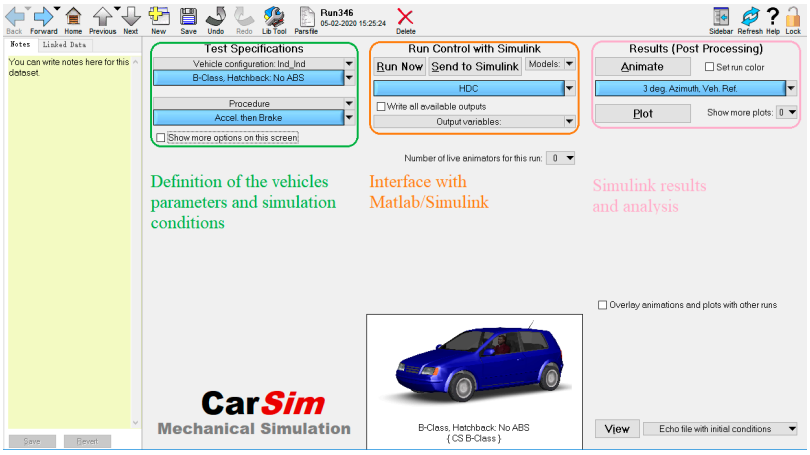

Figure 10. The CarSim user interface.

3.1. The Result Carried out with Fuzzy-PID Controller

The first test circumstance of simulation was set up in CarSim, and the slope of ramp was set as 20%, 40% and 15%, respectively. The vehicle accelerated from rest, and at the same time the HDC was requested. The test results are shown in Figure 11a–c, and the driver does nothing with the brake and acceleration pedals, the actual speed can follow the target speed well when the slope of the ramp is varied.

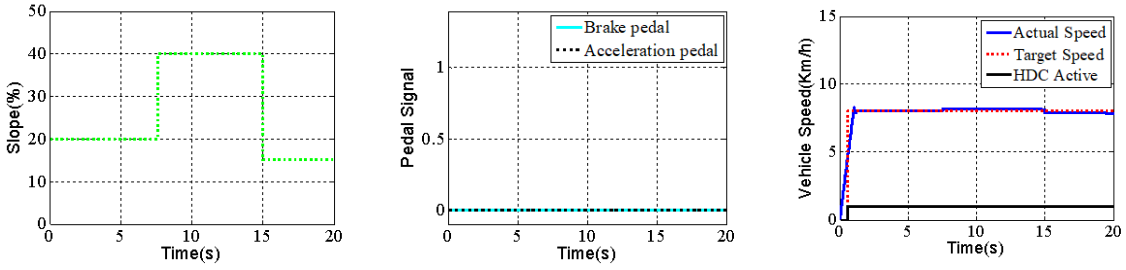

(**a**) (**b**) (**c**)

Figure 11. Slope of ramp (**a**), brake and acceleration pedals signal (**b**), actual speed and target speed of the vehicle (**c**), the result carried out with fuzzy-PID controller.

The second test circumstance of the simulation was set up in CarSim, the slope of ramp was constant with a value of 20%. The vehicle accelerated from rest, at the same time the HDC was

requested. During this process, the brake and acceleration pedal were pushed at random. The specific test results are shown in Figure 12a–c, and target speed decreases when the driver pushes the brake pedal and increases when the driver pushes the acceleration pedal. The results indicate that the actual speed has a good effect compared to the varied target speed.

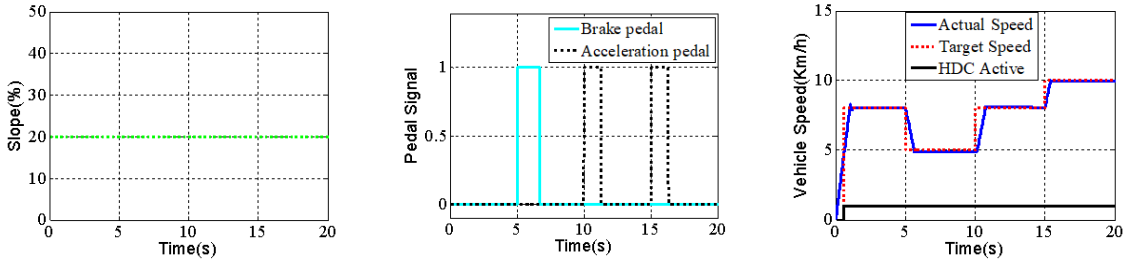

(**a**) (**b**) (**c**)

Figure 12. Slope of ramp (**a**), brake and acceleration pedals signal (**b**), actual speed and target speed of the vehicle (**c**), the result carried out with fuzzy-PID controller.

3.2. The Result Carried out with PID Controller

The same circumstance of simulation was set up in the CarSim and the operation of the car was the same as above. The test results are shown in Figures 13a–c and 14a–c:

We can see from the simulation result that the actual speed can follow the target speed well. However, the overshoot of PID controller and the time to reach steady state are greater than that of fuzzy-PID controller. The fuzzy-PID controller has a great advantage over PID controller.

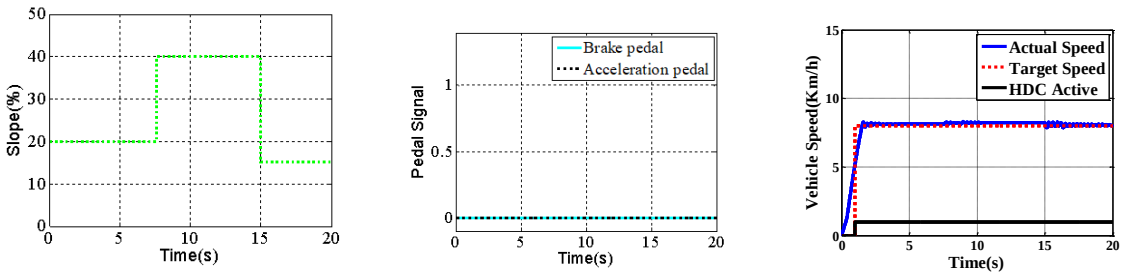

(**a**) (**b**) (**c**)

Figure 13. Slope of ramp (**a**), brake and acceleration pedals signal (**b**), actual speed and target speed of the vehicle (**c**), the result carried out with PID controller.

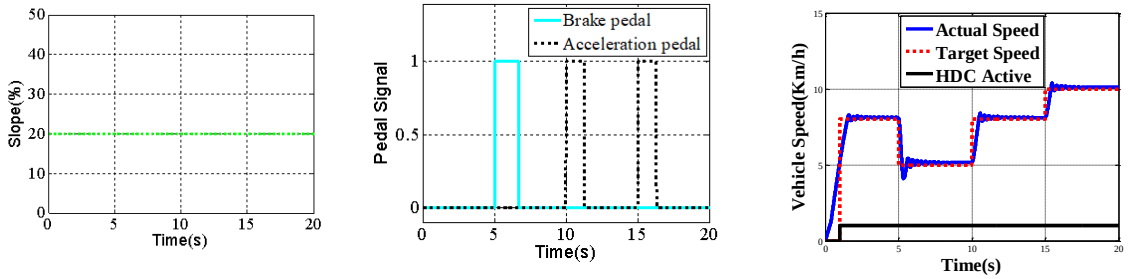

(**a**) (**b**) (**c**)

Figure 14. Slope of ramp (**a**), brake and acceleration pedals signal (**b**), actual speed and target speed of the vehicle (**c**), the result carried out with PID controller.

4. Real Vehicle Tests and Analysis

The control strategy of HDC was generated to be the code by the code generation tools of MATLAB/Simulink, and was integrated with existing ESP products. Then, we validated it in a real vehicle.

The structural explosion diagram of electronic control unit (ECU), hydraulic control unit (HCU) and real picture of ESP are shown in Figure 15. The image of the proving ground and the location of the ESP on the vehicle are shown in Figure 16.

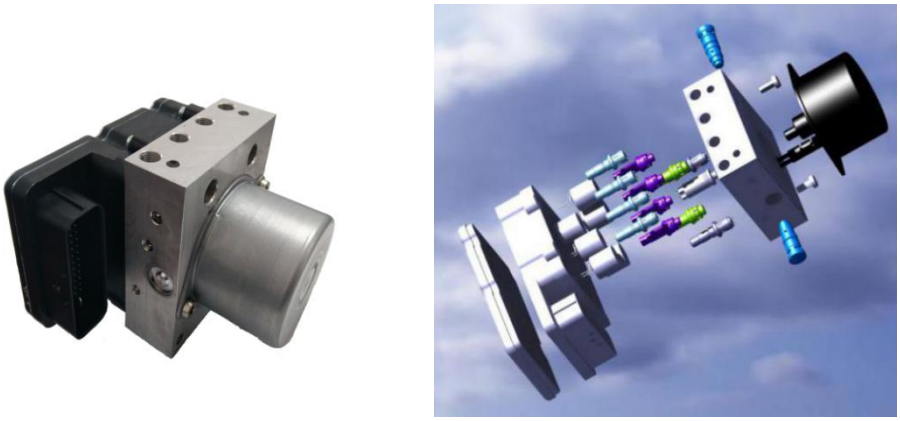

(**a**) (**b**)

Figure 15. Real figure of ESP (**a**), Structural explosion diagram of ESP (**b**).

(**a**) (**b**)

Figure 16. Proving ground and the vehicle (**a**), the location where the ESP is installed on the vehicle (**b**).

The physical effects of longitudinal acceleration are measured by the longitudinal acceleration sensor when the vehicle travels on the slope. From the operating principle, this acceleration consists of two parts, one of them is the component of gravity in the direction of the slope and the other can be expressed by the differential of the speed. It can be described as the following formula:

$$Ax = g \cdot \sin\theta + \dot{V}_{Act} \tag{10}$$

For small angles the angle, its sinus and its tangent, are the same. The real road slope is small, so the slope of the ramp can be calculated by the following formula:

$$\alpha = \frac{Ax - \dot{V}_{Act}}{g} \cdot 100\% \tag{11}$$

The meaning of the symbols in Formulas (10) and (11) are shown in Table 1.

The signal of vehicle speed, brake pedal and accelerator pedal are from the vehicle controller area network (CAN). The supervisory control and data acquisition are from Vector Tools.

The first test, drive the car to the ramp and push the HDC button (the HDC is requested when this button is pushed), release the brake and accelerator pedals. The test results are as follows:

As shown in Figures 17–19, the driver does nothing with the brake and acceleration pedals, and the actual speed can follow target speed well on the different slope of ramp, which are 10%, 15% and 20%, respectively. The results are consistent with the results of the Co-simulation.

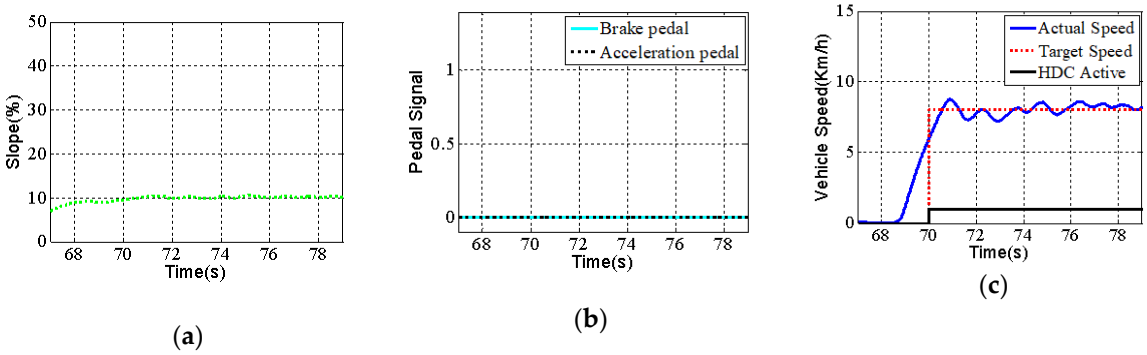

Figure 17. Slope of ramp (**a**), brake and acceleration pedals signal (**b**), actual speed and target speed of the vehicle (**c**), at the slope of 10% and the driver does nothing with the pedal.

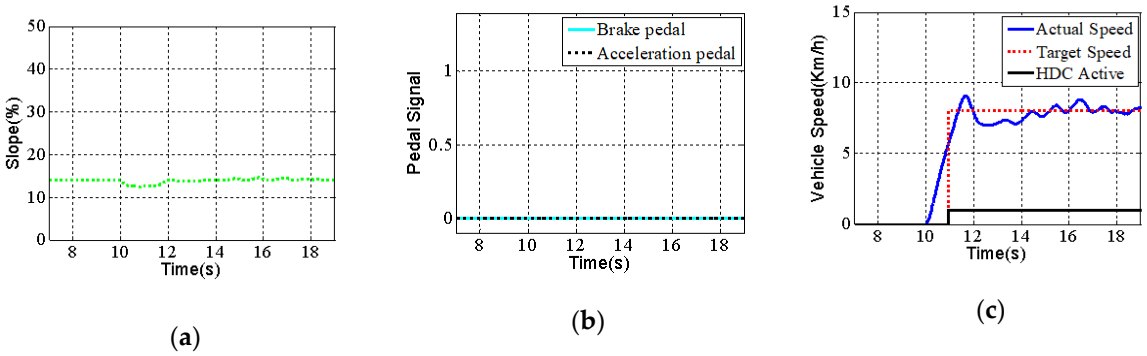

Figure 18. Slope of ramp (**a**), brake and acceleration pedals signal (**b**), actual speed and target speed of the vehicle (**c**), at the slope of 15% and the driver does nothing with the pedal.

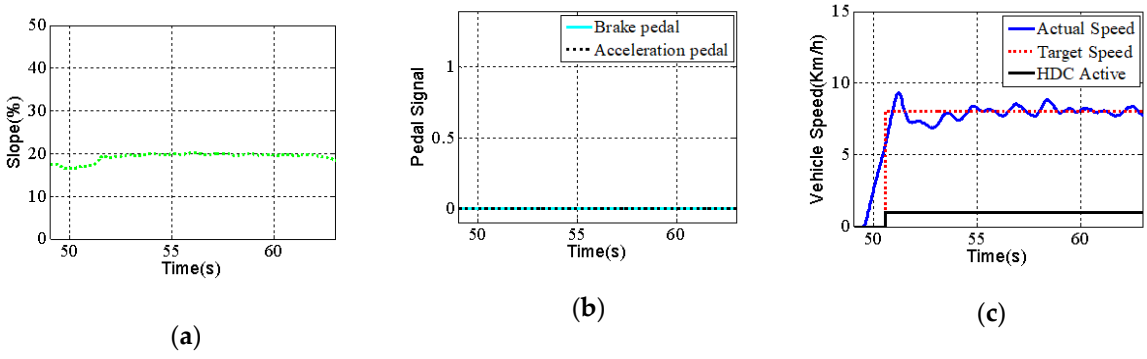

Figure 19. Slope of ramp **(a)**, brake and acceleration pedals signal (**b**), actual speed and target speed of the vehicle (**c**), at the slope of 20% and the driver does nothing with the pedal.

The second test, we drive the car to the ramp with slope is 20% and push the HDC button, and release the brake and accelerator pedals at the same time. When the vehicle speed is steady, the brake pedal will be pushed randomly. The test results are as follows:

As shown in Figure 20, target speed of vehicle decrease when the driver pushes the brake pedal. The results show that the actual speed has a better following effect than the varied target speed, which is consistent with the results of the co-simulation.

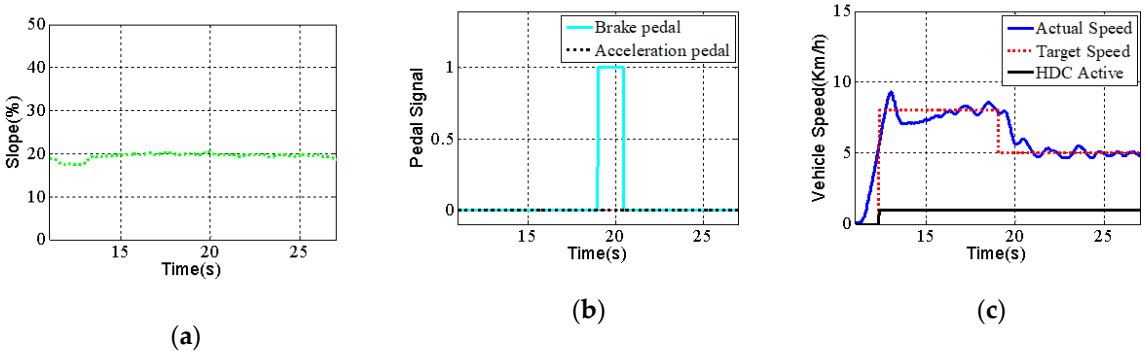

(**a**) (**b**) (**c**)

Figure 20. Slope of ramp (**a**), brake and acceleration pedals signal (**b**), actual speed and target speed of the vehicle (**c**), the vehicle at the slope of 20% and the driver pushes the brake pedal at random.

In the third test, we drove the car to the ramp with a slope of 20% and pushed the HDC button, and released the brake and accelerator pedals. The accelerator pedal was pushed randomly after the vehicle speed was steady. The test results are as follows:

As shown in Figure 21, the target speed of vehicle increases when the driver pushes the acceleration pedal. The results reveal that, compared to the varied target speed, the actual speed has a better following effect, which is consistent with the results of the co-simulation.

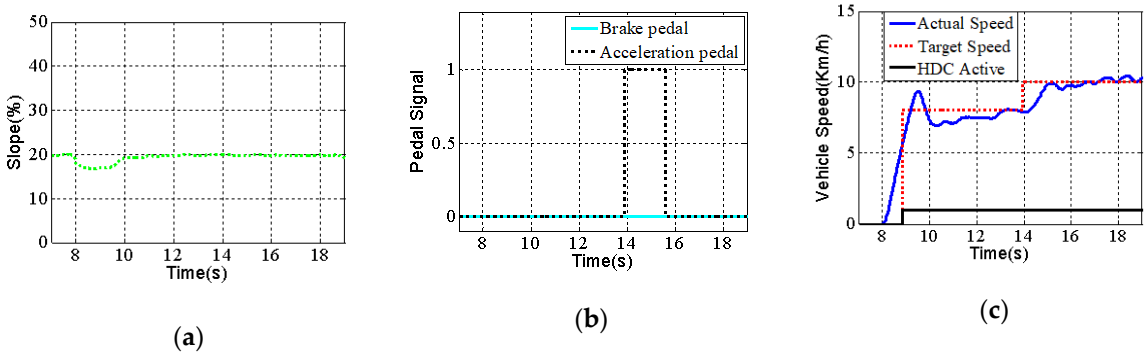

(**a**) (**b**) (**c**)

Figure 21. Slope of ramp (**a**), brake and acceleration pedals signal (**b**), actual speed and target speed of the vehicle (**c**), the vehicle at the slope of 20% and the driver pushes the acceleration pedal at random.

5. Conclusions

In order to reduce the workload of the driver during downhill, we explored an efficient vehicle HDC system based on ESP. In this work, both simulations and experiments were performed to validate the effectiveness of the proposed strategy. The experimental results show that both the overshoot and the time to reach a steady state of fuzzy PID are shorter than that of PID. The simulation and actual vehicle test results co-confirm that the vehicle can maintain very low speed, which is the varied target speed, during downhill driving whether it is a ramp change or driver intervention. Therefore, it is very reasonable for us to believe that the HDC is a feasible and effective system to assist the driver in controlling the vehicle speed during driving downhill. In addition, our system also improves the vehicle's safety and reduces the driver's workload.

Author Contributions: Conceptualization, L.J. and R.Z.; methodology, L.J. and R.Z.; software, R.Z. and H.G.; validation, L.J. and R.Z.; data curation, B.T. and H.G.; writing, R.Z.; supervision, B.T. and H.G.; project administration, L.J. and B.T. All authors have read and agreed to the published version of the manuscript.

Funding: This research received no external funding.

Conflicts of Interest: The authors declare no conflict of interest.

References

1. International Transport Forum. *Road Safety Annual Report*; OECD Publishing: Paris, France, 2017.
2. Orynycz, O.; Tucki, K.; Wasiak, A.; Sobótka, R.; Gola, A. Evaluation of the Brake's Performance Dependence Upon Technical Condition of Car Tires as a Factor of Road Safety Management. *Energies* **2020**, *13*, 9. [CrossRef]
3. Luo, Y.; Han, Y.; Chen, L.; Li, K. Downhill Safety Assistance Control for Hybrid Electric Vehicles based on the Downhill Driver's Intention Model. *Proc. Inst. Mech. Eng. D J. Automob. Eng.* **2015**, *229*, 1848–1860. [CrossRef]
4. Silyanov, V.V. Comparison of the pattern of accident rates on roads of different countries. *Traffic Eng. Control* **1973**, *14*, 432–435.
5. Zheng, S.Y.; Jin, C. Research on Engine Cranking Process in Downhill Braking Condition for an Electric Drive Underground Dump Truck. *Appl. Mech. Mater.* **2013**, *364*, 92–96. [CrossRef]
6. Konrad, R. *Automotive Mechatronics: Automotive Networking, Driving Stability Systems, Electronics*; Springer Vieweg: Wiesbaden, Germany, 2015; pp. 394–403.
7. Chen, J.; Liu, X.; Wang, T.; Gong, X.; Sun, H.; Wang, G.; Chen, W. Charging Valve of the full Hydraulic Braking System. *Adv. Mech. Eng.* **2016**, *8*, 1–11. [CrossRef]
8. Rumore, R. Considerations for diesel engine exhaust brakes. *Diesel Prog. N. Am. Ed.* **1998**, *64*, 40–41.
9. Senft, J.R. Brake power maxima of engines with limited heat transfer. *Energy Convers. Eng. Conf.* **1997**, *2*, 973–978.
10. Gotsch, D.A. New brake-retarder for heavy-duty trucks. *SAE* **1960**, *68*, 118–120.
11. Razmyslov, V.A.; Kuz'min, V.M.; Serikov, A.V. Calculations of braking force of electro-dynamical railway car retarder. *Russ. Electr. Eng.* **2008**, *79*, 280–282. [CrossRef]
12. Zhao, W.; Wu, G.; Wang, C.; Yu, L.; Li, Y. Energy transfer and utilization efficiency of regenerative braking with hybrid energy storage system. *J. Power Sources* **2019**, *427*, 174–183. [CrossRef]
13. Zheng, H.; Lei, Y.; Song, P. Design of a Filling ratio Observer for a Hydraulic Retarder: An Analysis of Vehicle Thermal Management and Dynamic Braking System. *Adv. Mech. Eng.* **2016**, *8*, 1–8. [CrossRef]
14. Nakawaki, Y.; Shindo, Y.; Higashiyama, Y. Apparatus for controlling engine brake force during vehicle running on downhill with released accelerator. U.S. Patent 5287773A, 22 February 1994.
15. Cummins, D.D. The Jacobs engine brake application and performance. In Proceedings of the SAE National Powerplant and Transportation Meetings, Chicago, IL, USA, 17–21 October 1966.
16. Faletti, J.J.; Feucht, D.D.; Hakkenberg, P. Simultaneous exhaust valve opening braking system. U.S. Patent 5526784A, 18 June 1996.
17. Göhring, E.; von Glasner, E.-C.; Povel, R. *Engine Braking Systems and Retarders—An Overview from an European Standpoint*; SAE International: Toledo, OH, USA, 1992.
18. Anwar, S. A parametric model of an eddy current electric machine for automotive braking applications. *IEEE Trans. Control Syst. Technol.* **2004**, *12*, 422–427. [CrossRef]
19. Kost, F.; Koch-Dücker, H.K.; Niewels, F.; Schuh, J.; Ehret, T.; Wagner, J.; Heinen, F.; Eberspächer, P. *Driving Stability Systems*; Robert Bosch GmbH: Plochingen, Germany, 2005; pp. 68–69.
20. Sahoo, B.P.; Panda, S. Improved grey wolf optimization technique for fuzzy aided PID controller design for power system frequency control. *Sustain. Energy Grids Netw.* **2018**, *16*, 278–299. [CrossRef]
21. Liu, Z.; Wan, R.; Shi, Y.; Chen, H. Simulation Analysis of Traction Control System for Four-Wheel-Drive Vehicle Using Fuzzy-PID Control Method. *Commun. Comput. Inform. Sci.* **2011**, *201*, 250–257.
22. Kazemian, H.B. Intelligent Fuzzy PID Controller: Applications of Fuzzy Control, Genetic Algorithms and Neural Networks. *Found. Gen. Optim.* **2008**, *2*, 241–260.
23. Pilla, R.; Azar, A.T.; Gorripotu, T.S. Impact of Flexible AC Transmission System Devices on Automatic Generation Control with a Metaheuristic Based Fuzzy PID Controller. *Energies* **2019**, *12*, 4193. [CrossRef]
24. Wu, X.; Xu, Y.; Liu, J.; Lv, C.; Zhou, J.; Zhang, Q. Characteristics Analysis and Fuzzy Fractional-Order PID Parameter Optimization for Primary Frequency Modulation of a Pumped Storage Unit Based on a Multi-Objective Gravitational Search Algorithm. *Energies* **2020**, *13*, 137. [CrossRef]

25. Croce, A.I.; Musolino, G.; Rindone, C.; Vitetta, A. Sustainable mobility and energy resources: A quantitative assessment of transport services with electrical vehicles. *Renew. Sustain. Energy Rev.* **2019**, *113*, e109236. [CrossRef]
26. Vuchic, V.R. *Urban Transit Systems and Technology*; John Wiley & Sons, Inc.: Hoboken, NJ, USA, 2007.
27. Ang, K.H.; Chong, G.; Yun, L. PID Control System Analysis, Design, and Technology. *IEEE Trans. Control Syst. Technol.* **2005**, *13*, 559–576.